



**HAL**  
open science

## Experimental OFDM transmission performance analysis in a SOA - fiber cavity laser

Raed El Hassanieh, Pascal Morel, Mohamad Hamze, Véronique Quintard,  
Andre Perennou, Ammar Sharaiha

► **To cite this version:**

Raed El Hassanieh, Pascal Morel, Mohamad Hamze, Véronique Quintard, Andre Perennou, et al..  
Experimental OFDM transmission performance analysis in a SOA - fiber cavity laser. Optics Express,  
2023, 31 (15), pp.24875. 10.1364/OE.494718 . hal-04211301

**HAL Id: hal-04211301**

**<https://hal.science/hal-04211301v1>**

Submitted on 19 Sep 2023

**HAL** is a multi-disciplinary open access archive for the deposit and dissemination of scientific research documents, whether they are published or not. The documents may come from teaching and research institutions in France or abroad, or from public or private research centers.

L'archive ouverte pluridisciplinaire **HAL**, est destinée au dépôt et à la diffusion de documents scientifiques de niveau recherche, publiés ou non, émanant des établissements d'enseignement et de recherche français ou étrangers, des laboratoires publics ou privés.



# Experimental OFDM transmission performance analysis in a SOA - fiber cavity laser

RAED EL HASSANIEH,<sup>1,2,\*</sup>  PASCAL MOREL,<sup>1</sup> MOHAMAD HAMZE,<sup>2</sup>  
VERONIQUE QUINTARD,<sup>1</sup>  ANDRE PERENNOU,<sup>1</sup>  AND AMMAR SHARAIHA<sup>1</sup>

<sup>1</sup>Ecole Nationale d'Ingénieurs de Brest (ENIB), CNRS, UMR 6285 Lab-STICC, 29238 Brest, France

<sup>2</sup>Arts Sciences and Technology University in Lebanon (AUL), Cola, Beirut, Lebanon

\*raed.al-hassanieh@enib.fr

**Abstract:** In this article, we present an experimental study of OFDM transmission using a specific bi-directional fiber cavity laser based on a semiconductor optical amplifier. We show that in the presence of sinusoidal modulation, its frequency response presents resonances relative to the optical cavity modes. We investigate first the performance of the system in terms of Error Vector Magnitude (EVM) for different configurations relative to the frequency position of the OFDM sub-carriers with respect to the frequency interval of the resonant modes. The obtained results show a significant improvement in the OFDM transmission EVM by increasing the OFDM subcarriers per frequency interval. We then analyze the impact of inter-symbol interference and inter-frame interference on the system's performance due to the round-trip echo and propose a pre-compensation method that added a small percentage of the previous symbol inverted before transmitting it inside the cavity where a decrease in the EVM is obtained respectively from 21.4% to 9.6% and from 26.8% to 13.2% for 4-QAM and 16-QAM data transmission.

© 2023 Optica Publishing Group under the terms of the [Optica Open Access Publishing Agreement](#)

## 1. Introduction

Several current research on Fiber Cavity Lasers (FCL) has been theoretically and experimentally explored with different architectures such as bidirectional or ring cavity architectures. In particular, bidirectional cavities have drawn significant attention due to their potential applications in Passive Optical Networks (PON) [1–3]. The ring cavity is another type of resonant cavity, which can be exploited for a variety of applications such as sensors [4,5]. Previous works have explored various aspects of fiber ring lasers based on RSOA, SOA, EDWA, and narrow-linewidth semiconductor technologies, providing valuable insights into stability, tunability, sensing applications, and wavelength switching capabilities [6–9]. Some applications require the transmission of data within the cavity itself. However, as the transmitted data makes multiple turns within the cavity, it creates residual modulation that leads to noise. Thus, selecting an appropriate cavity architecture becomes crucial in ensuring optimal transmission quality. Recent studies have been conducted on self-seeded cavities Reflective Semiconductor Optical Amplifier (RSOA) in PON applications since it ensures simultaneously amplifying and directly modulating data. Due to its non-linear behavior, the use of the RSOA, which is present at one end of the FCL, provides the data cancellation before one round trip in the cavity to encode new data onto the recirculating optical field [10,11]. Another approach consists of the use of a special mirror in the self-seeded cavity that averages the modulated signal and thus increases the quality of data transmission [12,13]. The same authors have recently proposed the use of passive modulation averaging for data erasure/modulation cancellation in PON [14].

In our work, we introduce a unique Semiconductor Optical Amplifier Fiber Cavity Laser (SOA-FCL) using specific bidirectional cavity architecture (Fig. 1) where light experiences bidirectional propagation along the fiber but unidirectional propagation in the Transmitter (Tx)

which will be described in the next section. This cavity structure not only reduces the laser noise and stabilizes the laser [15] but one can put the Transmitter and the Receiver (Rx) anywhere inside the cavity as a function of the network requirements. Also, we propose a customized modulation technique that is adapted based on the characterization of this unique FCL. This technique eliminates the need for additional devices to stabilize the cavity. Therefore, we analyze the SOA-FCL frequency response by modulating it, and we show that its frequency response presents resonance modes. To ensure the continuous transmission of data in this SOA-FCL, we use optical Orthogonal Frequency Division Multiplexing (OFDM) where we investigate first the performance of the system in terms of Error Vector Magnitude (EVM) for different configurations relative to the frequency position of the OFDM sub-carriers with respect to the frequency interval of the resonant modes. The EVM percentage is directly linked to the Bit Error Rate (BER) under gaussian noise assumption which provides a quantitative measure of the quality of the received signal and serves as an indicator of the system's performance [16]. By comparing the EVM to a predetermined threshold, we can assess the quality of the received signal. A lower EVM corresponds to a higher signal accuracy and, consequently, a lower BER. We then analyze the impact of inter-symbol interference and inter-frame interference on the system's performance due to the round-trip echo and propose a pre-compensation method by using the echo cancellation symbol method.

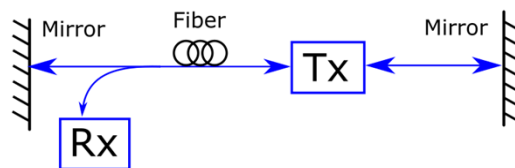


**Fig. 1.** Fiber Cavity Laser Schematic Diagram.

In this paper, we present in section 2 our experimental SOA-FCL structure and give its static characteristics and frequency response. section 3 is devoted to the description of the OFDM transmission configurations used within this FCL. Finally, section 4 is dedicated to the analysis of the data transmission for these different configurations using EVM measurements and discussing the results.

## 2. Fiber cavity laser

### 2.1. Cavity structure

The SOA-FCL structure depicted in Fig. 2 generates an optical wave by laser effect. Faraday rotators and Faraday mirrors are used to achieve polarization stability that can degrade the performance of the system as we use SMF fiber [1,17,18,19]. Although the cavity is considered to be bidirectional, the two circulators let the photons propagate only in one direction through the active elements (SOA and Mach-Zehnder modulator). This architecture prevents beating inside the SOA between the counterpropagating optical fields which leads to better stabilization inside the cavity. The cavity contains an Optical Bandpass Filter (OBPF) that selects a specific lasing wavelength range, also placed in one of the unidirectional paths to reduce losses.

In our setup, it is centered at 1550 nm with a flat bandwidth of 0.2 nm. Since the utilized SOA does not have a matched RF input, a Mach-Zehnder modulator (MZM) is inserted into the cavity to modulate the optical light. The MZM  $V_{\pi}$  is 2.3 V, and the  $V_{\text{bias}}$  is set to 4 V to achieve optimal modulation for data transmission. A Polarization Controller (PC) is also included to control and adjust the polarization state of the light which helps in optimizing the desired optical output power. The cavity length is increased by adding 120 m of Single Mode Fiber (SMF).

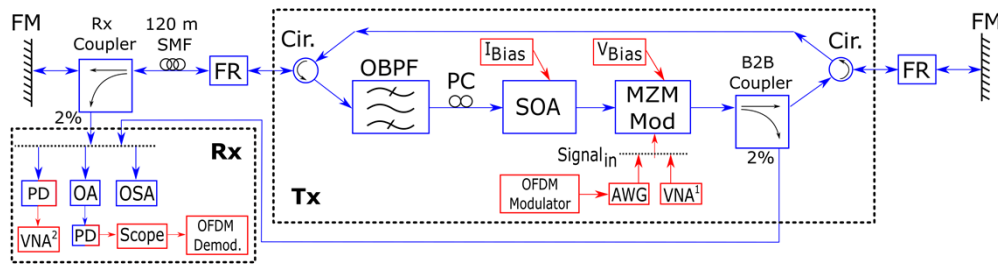


**Fig. 2.** Fiber Cavity Laser Experimental Structure. Blue color represents the optical path and components while red color represents the electrical ones. FM: Faraday Mirror; FR: Faraday Rotator; OBPF: Optical Bandpass Filter; PC: Polarization Controller; SOA: Semiconductor Optical Amplifier; MZM Mod: Mach-Zehnder Modulator; OA: Optical Amplifier; PD: photodiode; OSA: Optical Spectrum Analyzer; VNA: Vector Network Analyzer: 1 corresponds to port emitting sinusoidal signal and 2 corresponds to port receiving the transmitted signal; AWG: Arbitrary Waveform Generator.

Additionally, two couplers (98% / 2%) are used to analyze the transmitted signal where 98% of the optical power will continue propagating inside the cavity to maintain the resonance. The remaining 2% are taken outside the cavity to monitor optical output power at two different locations. The 1<sup>st</sup> coupler, denoted as the “B2B coupler”, is located directly after the MZM to analyze the cavity Back-to-back (B2B), while the 2<sup>nd</sup> coupler “Rx coupler” is located at the receiver side and is used to analyze the transmitted signal.

## 2.2. Static characteristics

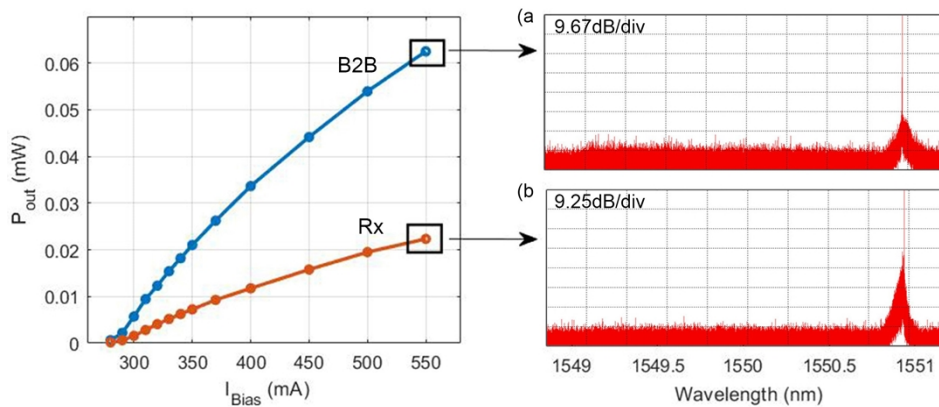


**Fig. 3.** Optical power at 2% coupler outputs (B2B and Rx) vs SOA bias current optical spectra for B2B (3a) and Rx (3b) at  $I_{bias}$  550 mA.

The relationship between the bias current ( $I_{bias}$ ) of the SOA and the output power ( $P_{out}$  taken at the coupler 2% output) of a FCL is described by the optical power versus current (P-I) curve as shown in Fig. 3. The P-I curve of our laser has a threshold of 280 mA and the output power increases rapidly with increasing the SOA bias current. In our experiment, the bias current is set to 550 mA to ensure maximal optical power. At this operating point, the obtained optical spectrum is shown in Fig. 3 for Tx and Rx locations. The optical spectrum displays a mono-mode laser in both cases (0.04 pm resolution). However, in the B2B analysis, the optical output power is observed to be around 4.3 dB higher. The noise floor in both cases stays more than 60 dB

below the peak power. Based on this value and taking into account the coupler ratio, the power inside the cavity can be estimated at around 3 mW at the B2B coupler and 1.1 mW at the Rx coupler. One should pay attention that the optical power inside the cavity can be also affected by the operating point of the Mach-Zehnder modulator. Here it's set to be optimal for further data transmission.

### 2.3. Cavity frequency resonant response

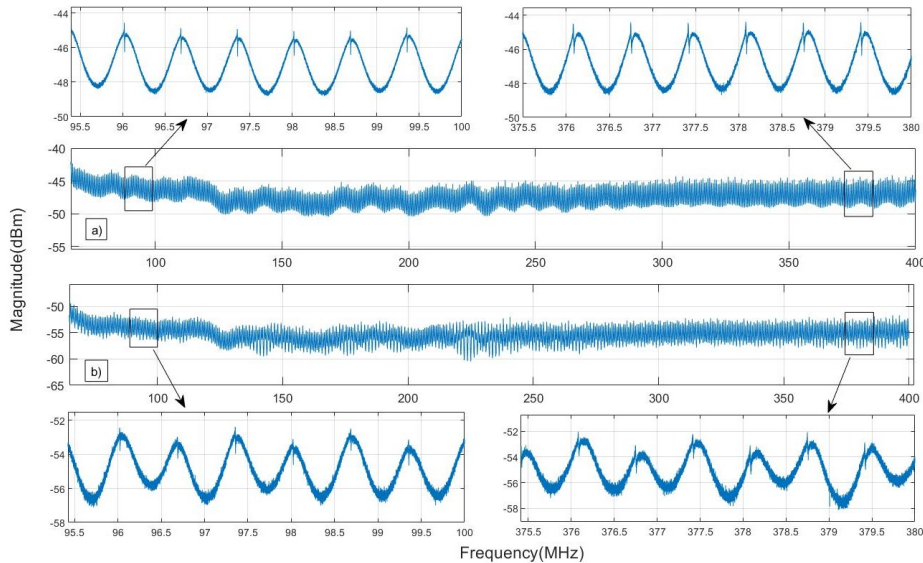


**Fig. 4.** Frequency Resonant Response measured by the VNA at B2B Coupler 2% output (4a) and at Rx Coupler 2% output (4b). FSR is measured to be equal to 0.666 MHz.

To achieve optimal data transmission, it is critical to determine the frequency response when the laser cavity is modulated. The cavity frequency response is obtained by using a Vector Network Analyzer (VNA) connected as shown in Fig. 2, sending a sweep of sine wave to the MZM and gathering the laser modulation response after photodetection. Figure 4 presents an example of the Frequency Resonant Response (FRR) of the laser cavity that can be determined by the length and the refractive index of the fiber of the SOA-FCL [20,21]. The frequency spacing between two resonant modes (FSR) is determined to be 0.666 MHz.

It is noteworthy that the amplitude and selectivity of the modes are directly related to the cavity's losses and gain. Hence, optimizing the MZM operating point and optical polarization is critical. It is worth noting that the Free Spectral Range (FSR) remains constant irrespective of the frequency range taken by the VNA or the optical output location inside the cavity. This is demonstrated in the zoomed insertions of Figs. 4(a) and (b).

## 3. Data transmission in a SOA-FCL

### 3.1. OFDM justification

OFDM is a multicarrier modulation technique that encodes modulated carriers with equal spacing to ensure orthogonality. In this paper we study OFDM implementation with an optical cavity that appears adapted to the presence of resonant modes as shown in the frequency cavity response in Fig. 4. We analyze the influence of the OFDM Sub-Carrier (SC) bandwidth concerning the cavity

FRR. Given the periodic modes present in the cavities, OFDM was chosen due to its advantageous features including robustness to frequency-selective fading, high spectral efficiency, mitigation of inter-symbol interference, flexibility in subcarrier allocation, and low implementation complexity [22–24].

The Intensity-Modulation Direct Detection (IMDD) technique is used to produce a real, positive signal from the OFDM transmitter [25]. The IMDD is characterized by its lower computing complexity and reduced cost in optical communication platforms. To initiate a genuine achievement from the transmitter, the Hermitian symmetry method is utilized [26].

### 3.2. OFDM configuration

As displayed in Fig. 5, OFDM SCs with data without a cyclic prefix are configured to be sent based on the Frequency Resonant Modes (FRM) enabling data transmission through the FCL in two different approaches. To discuss the efficiency of the OFDM transmission, different configurations are assessed for the OFDM frame construction to adapt each SC data bandwidth to the FRM bandwidth. The methodology was shown in our previous published paper [27] that was based on simulation study. However, in this paper, we assess the data transmission utilizing OFDM experimentally with different and more extensive approaches.

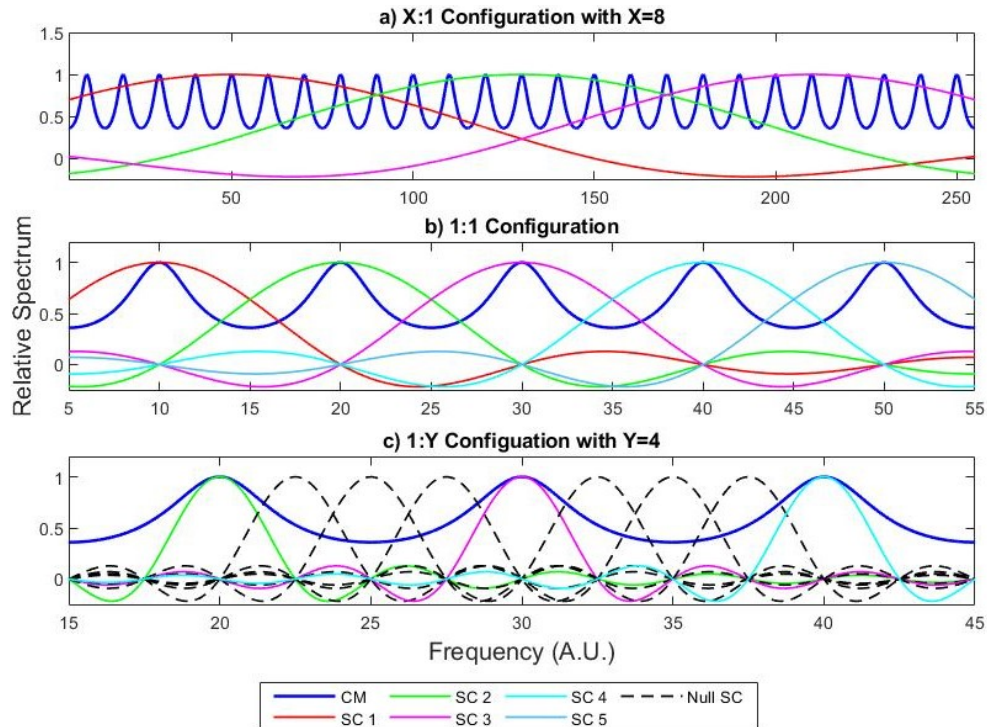


**Fig. 5.** OFDM SC covers more than one FRM. 5b. Every OFDM SC is located on one FRM. 5c. Three additional null SCs are added between the FRMs.

The first approach is to transmit data without taking into consideration the frequency response. In other words, every SC will cover more than one FRM as shown in Fig. 5(a) (X:1 configuration where X denotes the number of FRM in the main lobe of SC).

In the second approach, we have modified the number of the SC based on the FRM selectivity as shown in Fig. 5(c). In particular, the number of SCs is increased and only the SCs that match the modes would include data (1:Y configuration where Y denotes the number of active SC per

FRM). This approach enables the reduction of the SCs' bandwidth to be better adapted to the selectivity of the FRM. Finally, Fig. 5(b) shows a common data transmission technique where every SC is located on only one FRM.

Different X:1, 1:1, and 1:Y configurations of OFDM data transmission, shown in Table 1, are examined experimentally. These configurations depend on the FSR (0.666 MHz) being computed from the frequency response in section 2c. The first row in the table shows the FRM to SC ratio. In other words, X and Y correspond to the number of FRM and SC, respectively. Therefore, the two basic configurations will be X:1 where every SC might cover one or more FRMs. However, for the second configuration 1:Y, every FRM will contain one SC with the ability to insert null SC between two consecutive FRMs. For instance, 1:1 means that one FRM contains one SC. When the ratio is 16:1 that means every 16 FRMs are covered using one SC. However, to decrease the SCs bandwidth in the 1:2, 1:4, and 1:8, one, three, and seven null SCs are added between the FRM, respectively.

**Table 1. Transmission Parameters with OFDM Bandwidth of 341.4 MHz, Sampling Rate 11.949 GHz, Over-Sampling (OS) 35 and 16 Symbols/Frame. ISI: Inter-Symbol Interference. BR: Bit Rate.**

|                          |        |        |        |        |        |
|--------------------------|--------|--------|--------|--------|--------|
| X:1                      | 1:1    | 2:1    | 4:1    | 8:1    | 16:1   |
| SC per Symbol – FFT size | 512    | 256    | 128    | 64     | 32     |
| $\Delta f$ (MHz)         | 0.666  | 1.333  | 2.667  | 5.334  | 10.669 |
| BR (Mb/s)                | 677    | 672    | 661    | 640    | 597    |
| Symbol Duration $\mu s$  | 1478.5 | 739.25 | 369.63 | 184.81 | 92.41  |
| ISI %                    | 100    | 100    | 100    | 100    | 100    |
| 1:Y                      | 1:1    | 1:2    | 1:4    | 1:8    |        |
| SC per Symbol – FFT size | 512    | 1024   | 2048   | 4096   |        |
| $\Delta f$ (MHz)         | 0.666  | 0.333  | 0.166  | 0.0833 |        |
| BR (Mb/s)                | 603    | 301.5  | 151.75 | 75.375 |        |
| Symbol Duration $\mu s$  | 1.478  | 2.957  | 5.914  | 11.828 |        |
| ISI %                    | 100    | 50     | 25     | 12.5   |        |

In the X:1 configuration, the OFDM Symbol contains only 4 null SCs (1 at DC and 3 at the edges). However, in the 1:Y configuration, the OFDM symbol contains a different number of null SCs on the DC and Edges to have 452 Data SCs in all configurations. Each OFDM frame consists of 16 symbols and has a bandwidth of 341.4 MHz, derived from the number of SCs multiplied by the SC frequency spacing ( $\Delta f$ ). The terms  $\Delta f$  and BR values, mentioned in Table 1, represent the frequency spacing between OFDM SCs (FFT size) and the bit rate, respectively. ISI is Inter-Symbol Interference, which will be discussed in more detail in section 4. Also, the values of OFDM Bandwidth, Sampling Rate, Oversampling, and Symbols/Frame are found in the caption of Table 1.

#### 4. Results and discussion

To analyze the OFDM data transmission, the OFDM frame is first created and transferred to an Arbitrary Waveform Generator (AWG) to generate the time domain signal that will be the input of the MZM as shown in Fig. 2. A sampling rate of 11.949 GHz is selected to achieve an integer over-sampling (OS) factor of 35 at the emitter side. The 2% optical output is connected to an Optical Amplifier (OA) and then to a Photodiode (PD) converting the optical into an electrical signal. After that, the PD is connected to an oscilloscope for signal analysis with a sampling rate of 5 GSa/s limiting our bandwidth to 1.5 GHz, and the received signal is analyzed using

an OFDM receiver. Figure 6 shows the Error Vector Magnitude (EVM) and the constellation diagrams being examined after the OFDM receiver for the 1:Y configuration. The EVM value decreases from 20.7% to 8.8% between the 1:1 and 1:8 cases. Indeed, the constellation diagrams highlight a significant improvement while decreasing the SC bandwidth to fit the resonance selectivity of the cavity. It should be noted the close transmission performance between B2B and Rx, that will maintain all along the following results. This reveals that the Rx coupler can be placed anywhere inside the cavity without affecting the transmission performance.

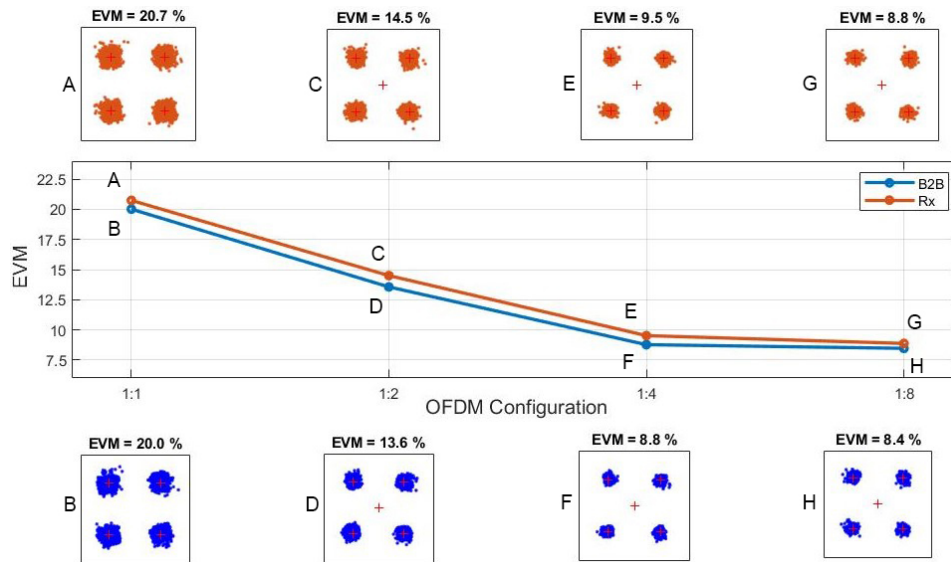


**Fig. 6.** EVM vs different OFDM configurations for 1:Y Ratios for the B2B and Rx and associated constellation diagrams.

However, when analyzing these results, the effect of Inter-Symbol Interference (ISI) and inter-frame interference (IFI) that occur in the cavity where the light will travel multiple times can be seen on the constellation diagrams. This leads to constructive and destructive interference of optical signals and can negatively affect the transmission quality, thus reducing the system's performance. Meanwhile, sent data is trapped inside the cavity and continue to travel from round trip to round trip with lower amplitudes as explained in Fig. 7. This phenomenon can be referred to as echo [10]. In this study, ISI occurs due to the overlapping of the echo from the previous symbol and the signal from the upcoming symbol, resulting in errors in the received signal. Setting the cyclic prefix to zero in all OFDM configurations allows an accurate analysis of the impact of ISI. This approach ensures that each symbol is precisely equivalent to an integer number of a round trip time, as induced by the link between the SC frequency spacing aligned on FRM and OFDM symbol duration, enhancing a more precise analysis of the echo effect. Table 1 also shows the relationship between the OFDM symbol duration, and the ISI percentage, where the number of round trips required to complete the transmission for one OFDM Symbol can be deduced based on the round trip duration of one photon. For instance, as shown in Fig. 7 when using a 1:1 configuration, the OFDM symbol duration is  $1.478 \mu\text{s}$ , which is equivalent to the time taken by a photon to complete a full round trip in the cavity, resulting in a 100% ISI. During the 2<sup>nd</sup> round trip, it is anticipated that the echo of the first symbol will undergo some reduction in amplitude, which will overlap with the second symbol. By the 3<sup>rd</sup> round trip, it is expected that the echo from the first symbol will become nearly insignificant, while the echo from the second symbol will overlap with the third symbol. In other words, the transmission is less sensitive to

ISI if the OFDM symbol duration is longer, therefore, part of the symbol will overlap with the echo which increases the transmission performance.

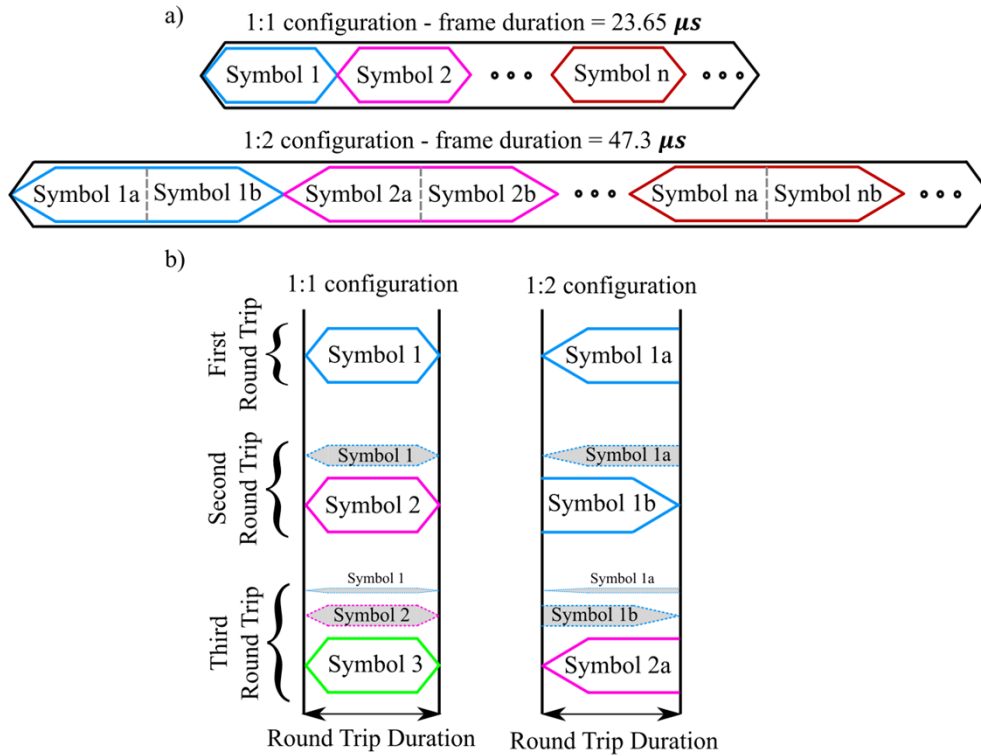


**Fig. 7.** Echo effect for 1:1 and 1:2 configurations. Symbols with gray backgrounds correspond to echoes from previous round trips. In the 1:2 configuration, symbol 1 can be artificially decomposed into 2 identical symbols, 1a and 1b, each having a duration equal to the round trip duration.

Figure 8 presents the transmission performance of configurations 1:1 to 16:1 where the presence of ISI effects from the echo is clearly shown, as they account for 100% of ISI, which in turn results in a rise in the EVM to reach around 21.4%. In contrast, for the 16:1 specific configuration, the duration of the frame (16 symbols/frame) matches the time for one round trip, resulting in 100% of constructive ISI since the frame is automatically repeated by the AWG, and consequently, this results in a decrease in the EVM. Therefore, if the OFDM symbol duration is shorter, the transmission’s sensitivity to ISI remains the same. By employing these X:1 configurations, a more precise examination of the effects of interference on data transmission becomes feasible. In open area transmissions, Cyclic-Prefix (CP) OFDM is designed and known to overcome ISI effects. In our experiment, the implementation of such CP-OFDM would yield improved results only if a 100% of CP ratio is added for a 1:1 configuration. This results in the reduction of the EVM from 21.4% to 8.9% for 4-QAM and from 26.8% to 11% for 16-QAM.

In the 1:Y configurations, the BR is reduced by half with every increase in Y (Table 1). In order to maintain the BR, processing techniques can be used, by correcting or reducing the impact of the echo as the cavity response can be thought of as an attenuated and delayed copy of the sent signal. A new OFDM configuration is then implemented to take into account this knowledge of the cavity response and eliminate the previous symbol’s echo by adding a small percentage of the previous symbol inverted before transmission. This ratio is denoted by “r” and the echo

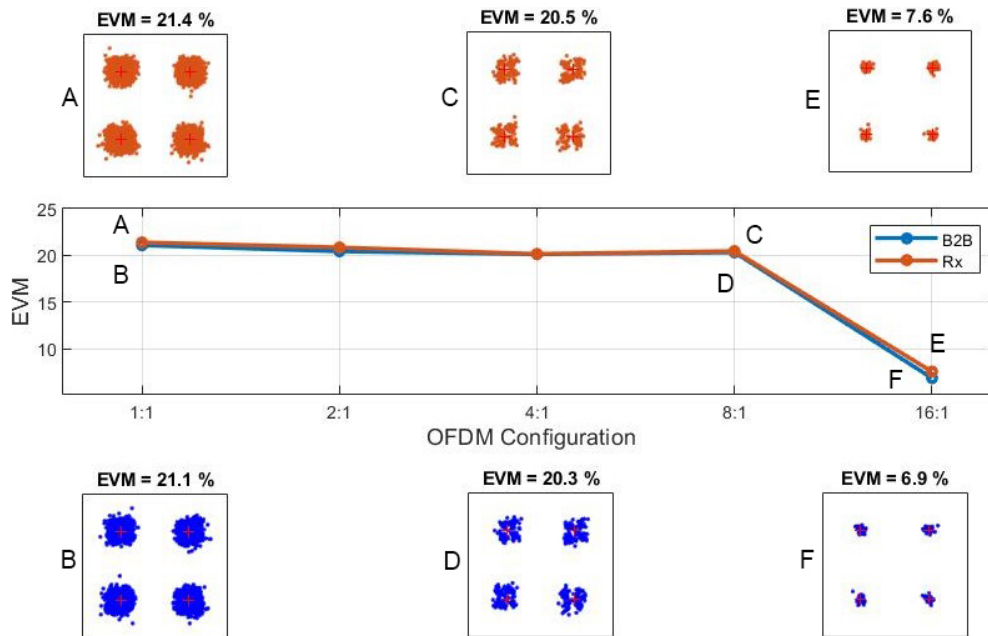


**Fig. 8.** EVM vs different OFDM configurations for X:1 Ratios for the B2B and Rx and associated constellation diagrams.

cancelation is achieved using the following equation:

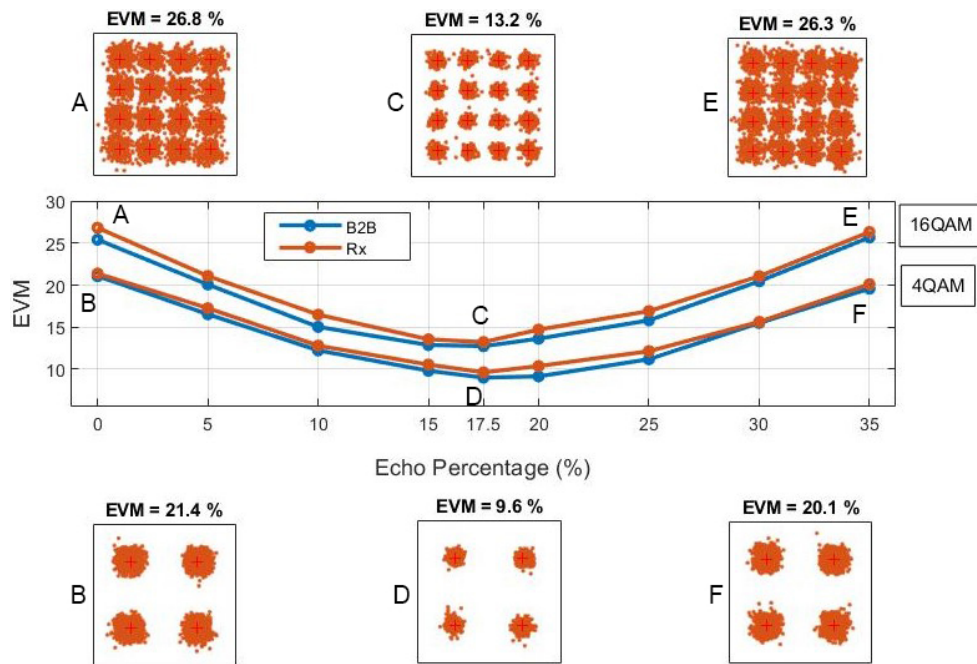
$$Symbol_{n,PreEcho} = Symbol_n - r \times Symbol_{n-1} \tag{1}$$

Figure 9 shows the EVM as a function of the echo pre-compensation ratio in the 1:1 configuration. We can see that an optimal value is attained for a ratio of about 17.5% for both, 4-QAM and 16-QAM. At  $r = 0\%$  (equal to 1:1 configuration in Fig. 6) the EVM exhibits a value of 21.4% for 4-QAM and 26.8% for 16-QAM, whereas after incorporating the echo cancelation mechanism and setting  $r$  to 17.5%, the EVM exhibits a value of 9.6% for 4-QAM and 13.2% for 16-QAM. We see the decisive contribution of the proposed method which leads to a consequent reduction of the EVM without losing BR.

A summary of the results obtained from the four methods employed in this study are shown in Table 2, which has been included to provide a clear and concise overview of the findings. Furthermore, it is important to note that all the results have been derived from the Rx during the transmission of OFDM signals utilizing a 4-QAM modulation format.

**Table 2. Summary of Rx Results when transmitting OFDM using 4-QAM Modulation Format.**

|                                |                           |      |      |      |      |
|--------------------------------|---------------------------|------|------|------|------|
| Configuration 1:Y - CP 0%      | 1:1                       | 1:2  | 1:4  | 1:8  | 1:16 |
|                                | EVM %                     | 20.7 | 14.5 | 9.5  | 8.8  |
| Configuration X:1 - CP 0%      | 1:1                       | 2:1  | 4:1  | 8:1  | 16:1 |
|                                | EVM %                     | 21.4 | 20.9 | 20.2 | 20.5 |
| Pre-echo Cancelation % - CP 0% | 0                         | 10   | 17.5 | 25   | 38   |
|                                | Configuration 1:1 - EVM % | 21.4 | 12.8 | 9.6  | 12.2 |
| Configuration X:1 - CP 100%    | 1:1                       | -    | -    | -    | -    |
|                                | EVM %                     | 8.9  | -    | -    | -    |



**Fig. 9.** EVM vs echo pre-compensation ratio for 1:1 configuration in the case of 4-QAM and 16-QAM. Constellation diagrams are shown for  $r = 0\%$ ,  $17.5\%$  and  $35\%$ .

## 5. Conclusion

In this study, we investigated a specific bidirectional SOA-FCL architecture cavity using OFDM transmission. The results showed the possibility of using OFDM data transmission in our laser cavity after analyzing, experimentally, the impact of the position of OFDM SCs with respect to the observed resonance modes on the frequency response. The EVM and constellation diagrams demonstrated that the self-seeded FCL approach could significantly improve the OFDM transmission performance, especially when modifying the number of the SC based on the FRM selectivity. Also, we investigated the impact of echo in a FCL cavity. The results showed that the echo has a significant effect on the system's performance, leading to increased ISI and IFI, which ultimately results in a higher EVM. To mitigate this effect, a new OFDM configuration was proposed that added a small percentage of the previous symbol inverted before transmitting it inside the cavity. This approach resulted in a considerable improvement in the constellation diagrams and a decrease in the EVM of approximately 12% from 21.4% and 14% from 26.8% for 4 and 16-QAM respectively. Furthermore, it is worth noting that the methods proposed in this study hold the potential to be applied to higher order M-QAM formats, enabling increased data rates, and further improving the overall system performance. Overall, the findings of this study demonstrated the importance of considering echo and suggested effective approaches to mitigate its impact on system performance. Our study provided insights into the use of self-seeded FCL cavities for optical OFDM transmission that would open the way for future research. Also, it would be interesting to optimize the coupler ratio to have the best compromise between transmission efficiency within the cavity and SNR ratio at the receiver.

**Funding.** Conseil Départemental du Finistère; Brest Métropole; Arts, Sciences and Technology University in Lebanon.

**Disclosures.** The authors declare no conflicts of interest.

**Data availability.** The data underlying the results presented in this study are not publicly available at this time but may be obtained from the authors upon reasonable request.

## References

1. S. A. Gebrewold, L. Marazzi, P. Parolari, R. Brenot, SPÓ Dúill, R. Bonjour, D. Hillerkuss, C. Hafner, and J. Leuthold, "Reflective-SOA Fiber Cavity Laser as Directly Modulated WDM-PON Colorless Transmitter," *IEEE J. Quantum Electron.* **20**(5), 503–511 (2014).
2. F. Saliou, G. Simon, P. Chanclou, M. Brunero, L. Marazzi, P. A. O. L. A. Parolari, M. Martinelli, R. Brenot, A. Maho, S. Barbet, and G. Gavioli, "125-km Long Cavity Based on Self-Seeded RSOAs Colorless Sources for 2.5-Gb/s DWDM Networks," *J. Lightwave Technol.* **33**(8), 1602–1607 (2015).
3. S.D. Le, Q. Deniel, F. Saliou, A., Lebreton, and P. Chanclou, "16×2.5 Gbit/s and 5 Gbit/s WDM PON based on self-seeded RSOA," *2013 15th International Conference on Transparent Optical Networks (ICTON)*, Cartagena, Spain, 1–4 (2013).
4. C.H. Yeh, H.Z. Chen, J.Y., Chen, and C.W. Chow, "Utilizing New Erbium-Doped Fiber Laser Scheme for Long-Distance Fiber Bragg Grating (FBG) Sensor System," *IEEE Sensors*, 1–3 (2015).
5. Q. Fu, Y. Li, J., Tian, and Y. Yao, "Dual-channel fiber ultrasonic sensor system based on fiber Bragg grating in an erbium-doped fiber ring laser," *IEEE 2017 Conference on Lasers and Electro-Optics Pacific Rim (CLEO-PR)*, 1–3 (2017).
6. C. H. Yeh, J. Y. Sung, L. G. Yang, C. W. Chow, and J. H. Chen, "Stable and wavelength-tunable RSOA-and SOA-based fiber ring laser," *Opt. Fiber Technol.* **20**(3), 250–253 (2014).
7. P. C. Peng, K. M. Feng, W. R. Peng, H. Y. Chiou, CC, Chang, and S. Chi, "Long-distance fiber grating sensor system using a fiber ring laser with EDWA and SOA," *Opt. Commun.* **252**(1-3), 127–131 (2005).
8. Y. W. Lee, J. Jung, and B. Lee, "Multiwavelength-switchable SOA-fiber ring laser based on polarization-maintaining fiber loop mirror and polarization beam splitter," *IEEE Photonics Technol. Lett.* **16**(1), 54–56 (2004).
9. Z. Hu, F. Li, Z. Pan, and W. Tan, "Wavelength-tunable narrow-linewidth semiconductor fiber-ring laser," *IEEE Photonics Technol. Lett.* **12**(8), 977–979 (2000).
10. S. A. Gebrewold, R. Bonjour, S. Barbet, A. Maho, R. Brenot, P. Chanclou, M. Brunero, L. Marazzi, P. Parolari, A. Totovic, and D. Gvozdic, "Self-Seeded RSOA-Fiber Cavity Lasers vs. ASE Spectrum-Sliced or Externally Seeded Transmitters—A Comparative Study," *Appl. Sci.* **5**(4), 1922–1941 (2015).
11. M. L. Deng, B. Y. Cao, R. P. Giddings, Y. X. Dong, N. Jiang, D. Nettet, K. Qiu, and J. M. Tang, "Intra-Cavity Chromatic Dispersion Impacts on 10-Gb/s Optical OFDM Transmissions Over 25-km Dual-RSOA-Based Self-Seeded PON Systems," *IEEE Photonics J.* **7**(1), 1–12 (2015).
12. M. Šprem, T. Komljenović, D., Babić, and Z. Šipuš, "Colorless optical sources for fiber-optic access networks of new generation," *Proceedings ELMAR-2014. IEEE*, 1–4 (2014).
13. T. Komljenovic, D. Babić, and Z. Sipus, "47-km 1.25-Gbps transmission using a self-seeded transmitter with a modulation averaging reflector," *Opt. Express* **20**(16), 17386–17392 (2012).
14. M. Šprem and D. Babić, "Wavelength reuse WDM-PON using RSOA and modulation averaging," *Opt. Commun.* **451**, 1–5 (2019).
15. R. El Hassanieh, P. Morel, M. Hamze, V. Quintard, A. Pérennou, and A. Sharaiha, "Time Domain Numerical Study of Two Semiconductor Optical Amplifiers Laser Cavity Structures," *2021 International Conference on Numerical Simulation of Optoelectronic Devices (NUSOD)*, 123–124 (2021).
16. R. Schmogrow, B. Nebendahl, M. Winter, A. Josten, D. Hillerkuss, S. Koenig, J. Meyer, M. Dreschmann, M. Huebner, C. Koos, and J. Becker, "Error Vector Magnitude as a Performance Measure for Advanced Modulation Formats," *IEEE Photonics Technol. Lett.* **24**(1), 61–63 (2012).
17. M. Martinelli, L. Marazzi, P. Parolari, M. Brunero, and G. Gavioli, "Polarization in Retracing Circuits for WDM-PON," *IEEE Photonics Technol. Lett.* **24**(14), 1191–1193 (2012).
18. M. Gay, L. Bramerie, K. Hussain, T. Chartier, S. Trebaol, J. C. Simon, A. Maho, and R. Brenot, "Enhanced Amplitude Noise Tolerance of a Self-Seeded RSOA Laser Using Balanced Detection," *IEEE Photonics Technol. Lett.* **29**(24), 2219–2221 (2017).
19. S.A. Gebrewold, L. Marazzi, P. Parolari, M. Brunero, R. Brenot, D. Hillerkuss, C., Hafner, and J. Leuthold, "Colorless self-seeded fiber cavity laser transmitter for WDM-PON," *2014 Conference on Lasers and Electro-Optics (CLEO) - Laser Science to Photonic Applications*, San Jose, CA, USA, 1–2 (2014).
20. A. Maho, G. Simon, S. Barbet, F. Lelarge, F. Saliou, P. Chanclou, P. Parolari, L. Marazzi, M. Brunero, M. Martinelli, and S. A. Gebrewold, "Demystification of the Self-Seeded WDM Access," *J. Lightwave Technol.* **34**(2), 776–782 (2016).
21. C. R. Doerr, "Direct modulation of long-cavity semiconductor lasers," *J. Lightwave Technol.* **14**(9), 2052–2061 (1996).
22. S. Cioni, G.E. Corazza, M., Neri, and A. Vanelli-Coralli, "OFDM vs. HSDPA comparison for satellite digital multimedia broadcasting systems," *GLOBECOM '05. IEEE Global Telecommunications Conference*, (2005).
23. U. Berthold, F. K. Jondral, S. Brandes, and M. Schnell, "OFDM-Based Overlay Systems: A Promising Approach for Enhancing Spectral Efficiency [Topics in Radio Communications]," *IEEE Commun. Mag.* **45**(12), 52–58 (2007).
24. A. M. Jaradat, JM, Hamamreh, and H. Arslan, "OFDM With Subcarrier Number Modulation," *IEEE Wireless Commun. Lett.* **7**(6), 914–917 (2018).

25. N.E. Jolley, H. Kee, P. Pickard, J., Tang, and K. Cordina, "Generation and propagation of a 1550 nm 10 Gbit/s optical orthogonal frequency division multiplexed signal over 1000 m of multimode fibre using a directly modulated DFB," *OFC/NFOEC Technical Digest. Optical Fiber Communication Conference* 6, 3 (2005).
26. H., Lin and P. Siohan, "OFDM/OQAM with Hermitian Symmetry: Design and Performance for Baseband Communication," *2008 IEEE International Conference on Communications*, Beijing, China, 652–656 (2008).
27. R. El Hassanieh, P. Morel, M. Hamze, V. Quintard, A. Pérennou, and A. Sharaiha, "OFDM Transmission Using a Self-seeded Ring Cavity Based on a Semiconductor Optical Amplifier," *2022 International Conference on Numerical Simulation of Optoelectronic Devices (NUSOD)*, Turin, Italy, 31–32 (2022).